Chemical Research in Toxicology®

Article

Dose-dependent response to 3-nitrobenzanthrone exposure in human urothelial cancer cells

Mario Pink, Nisha Verma, Anna Zerries, and Simone Schmitz-Spanke

Chem. Res. Toxicol., **Just Accepted Manuscript** • DOI: 10.1021/acs.chemrestox.7b00174 • Publication Date (Web): 18 Sep 2017

Just Accepted

ACS Publications

Chemical Research in Toxicology is published by the American Chemical Society.
1155 Sixteenth Street N.W., Washington, DC 20036

Dose-dependent response to 3-nitrobenzanthrone exposure in human urothelial cancer cells

Mario Pink[a,b,], Nisha Verma[a], Anna Zerries[a], and Simone Schmitz-Spanke[a]*

[a] Institute and Outpatient Clinic of Occupational, Social and Environmental Medicine, University of Erlangen-Nuremberg, Schillerstr. 25/29, 91054 Erlangen, Germany

[b] Postgraduate Course for Toxicology and Environmental Toxicology, Institute for Legal Medicine, University of Leipzig, Johannisallee 28, 04103 Leipzig, Germany

*Corresponding author
Mario Pink, Institute and Outpatient Clinic of Occupational, Social and Environmental Medicine, University of Erlangen-Nuremberg, Schillerstraße 25/29, D-91054 Erlangen, Germany
E-mail: mario.pink@fau.de
Phone: +49-9131-8526102

Running Title: 3-nitrobenzanthrone and bladder cancer

Keywords: 3-nitrobenzanthrone (3-NBA); bladder toxicity; bioactivation; metabolomic profiling; adaptive response

ABSTRACT

A product of incomplete combustion of diesel fuel, 3-nitrobenzanthrone (3-NBA), has been classified as a cancer-causing substance. It first gained attention as a potential urinary bladder carcinogen due to the presence of its metabolite in urine and formation of DNA adducts. The aim of the present study was to characterise the dose-response relationship of 3-NBA in human urothelial cancer cell line (RT4) exposed to concentrations ranging from 0.0003 μM (environmentally relevant) to 80 μM by utilising toxicological and metabolomic approaches.

We observed that the RT4 cells were capable of bioactivation of 3-NBA within 30 minutes of exposure. Activity measurements of various enzymes involved in the conversion of 3-NBA in RT4 cells demonstrated NAD(P)H:quinone oxidoreductase (NQO1) as the main contributor for its bioactivation. Moreover, cytotoxicity assessment exhibited an initiation of adaptive mechanisms at low dosages, which diminished at higher doses, indicating that the capacity of these mechanisms no longer suffices - resulting in increased levels of intracellular reactive oxygen species, reduced proliferation and hyperpolarisation of the mitochondrial membrane.

To characterise the underlying mechanisms of this cellular response, the metabolism of 3-NBA and metabolomic changes in the cells were analysed. The metabolomic analysis of the cells (0.0003, 0.01, 0.08, 10, and 80 μM 3-NBA) showed elevated levels of various antioxidants at low concentrations of 3-NBA. Whereas, at higher exposure concentrations, it appeared that the cells reprogrammed their metabolism to maintain the cell homeostasis via activation of pentose phosphate pathway (PPP).

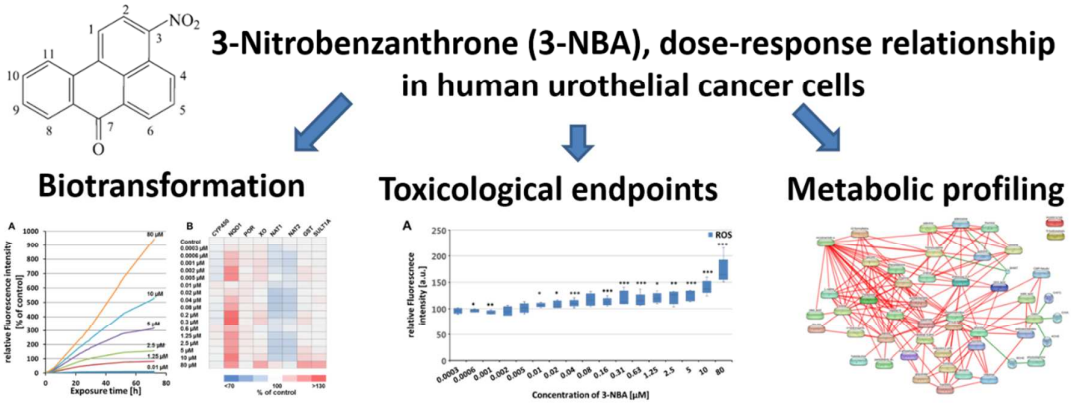

Table of content

INTRODUCTION

Exposure to environmental and occupational contaminants has long been known to be attributed to different kinds of life-threatening diseases. Bladder cancer is a classic example of such diseases, with studies reporting occupational exposure as the primary cause of approximately 5 to 25% of different kinds of bladder tumours.[1] Smoking and exposures to aromatic amines are well-known risk factors, however, different studies have also reported the potential of combustion products as a possible contributor to bladder cancer development.[2–7]

3-nitrobenzanthrone (3-nitro-7H-benz[de]anthracen-7-one, 3-NBA), a nitro-polycyclic aromatic hydrocarbon, has attracted a lot of attention due to its high genotoxic and mutagenic potential.[8–13] Although present only in minute quantities in diesel exhaust particles (0.647 – 6.61 μg/g), it induced the highest number of revertants per nanomole in the Ames test, that has been reported to date.[14] Moreover, the mechanistic data on the effects of 3-NBA lead to its classification as a possible human carcinogen (Group 2B) by the International Agency for Research on Cancer.[15]

Bound to diesel exhaust particles, the primary route of exposure to 3-NBA is via the respiratory tract. However, formation of DNA adducts after 3-NBA exposure in secondary organs of rodents with a particularly increased mutant frequency in urinary bladder have also been reported.[12] Biomonitoring studies of the urine of mine workers occupationally exposed to diesel emissions also demonstrated the presence of a minute quantity of 3-aminobenzanthrone (3-ABA), the main metabolite of 3-NBA.[16]

Keeping in mind that 3-NBA exerts a mutagenic effect in the bladder and the appearance of a urinary metabolite that can be oxidised to a reactive intermediate, the objective of the current study was to elucidate the mechanism of 3-NBA-induced bladder toxicity. Human bladder cancer epithelial cells (RT4 cell line) were exposed to environmentally relevant doses of 3-NBA, inter alia 0.0003 μM, the similar concentration of 3-ABA found in the 24 h urine of exposed mine workers.[16]

To elucidate the dose-dependent response of 3-NBA in the bladder, we studied its uptake and bioactivation, cytotoxicity, and finally its potential to alter the cellular metabolism RT4 cells. With the present work, we shed light on the cellular and metabolic response, highlighting the transition from an adaptive, respectively controlled state, to a repair and protection mode (maintaining homeostasis), to adverse effects that the cells undergo when exposed to 3-NBA.

MATERIALS AND METHODS

Chemicals and Reagents

Standard chemicals for cell culture (culture medium, foetal calf serum, supplements) were purchased from c.c.pro (Oberdorla, Germany). Chemicals for the synthesis of 3-NBA were purchased from Sigma-Aldrich (Steinheim, Germany), Merck Millipore (Darmstadt, Germany) and Alfa Aesar (Karlsruhe, Germany). The required chemicals for the metabolic assays were purchased from Alfa Aesar (Karlsruhe, Germany), Sigma-Aldrich (Steinheim, Germany) and Carl Roth (Karlsruhe, Germany). Fluorescence probes and chemicals for the toxicity assays were purchased from Life Technologies (Darmstadt, Germany), Promega (Mannheim, Germany), Santa Cruz Biotechnologie (Heidelberg, Germany) and Alfa Aesar (Karlsruhe, Germany). Solvents for extraction of intermediates of energy metabolism and required derivatisation agents were purchased from Merck Millipore (Darmstadt, Germany) and Sigma-Aldrich (Steinheim, Germany). All chemicals used were of analytical grade.

Cell culture

The human bladder cancer cell line RT4 (obtained from ATCC, Cat. No. ATCC® HTB-2™) was cultured until confluence in McCoy's 5A medium, supplemented with 10 % foetal bovine serum, 7.4 mg/mL L-glutamine (0.75 %), 100 units/mL penicillin, and 100 mg/mL streptomycin at 37°C in an atmosphere of 95% air and 5% CO_2.

The assays were performed in 96-well plates two days after seeding of 20,000 cells per well. The exposure was performed by incubation with culture medium containing 3-NBA (the concentration ranged from 0.3 nM to 10 µM) dissolved in DMSO (<0.1 % of the final concentration) for 24 hours. The same percentage of DMSO was used to expose control cells in all experiments. All experiments were performed at least five times in independent runs unless otherwise stated.

Synthesis of 3-NBA

3-NBA was synthesised by the nitration of benzanthrone. The first step of the synthesis was to dissolve benzanthrone (2.5 g, 10.8 mM) in nitrobenzene (30 mL). Then, concentrated nitric acid (4.0 mL) was added and the mixture was stirred at 40-50°C for 3h. Crude 3-NBA precipitated as a yellow solid from the cold reaction mixture and was recrystallised from glacial acetic acid. The purity of the product (98.8%) was determined by GC-MS.

Metabolic assays

Uptake and metabolic activation of 3-NBA to 3-ABA

The uptake and metabolic conversion of the non-fluorescent 3-NBA were monitored based on the fluorescence of 3-ABA.[17,18] 3-ABA emitted fluorescence was measured at a wavelength of 620 nm when excited at 470 nm. Fluorescence was monitored over a time span of 30 minutes to 72 h. Cells treated with normal cell culture medium were used to correct for auto-fluorescence of the cells. In addition, spontaneous formation of 3-ABA was monitored in a cell-free environment.

Determination of the catalytic activities of phase I and II biotransformation enzymes.

Catalytic activities of the following enzymes were measured: cytochrome P450 (CYP450), glutathione S-transferase (GST), two N-acetyltransferase isozymes (NAT1 & NAT2, sulfotransferase 1A1 (SULT1A), xanthine oxidase (XO), cytochrome P450 oxidoreductase (POR), and NAD(P)H:quinone oxidoreductase (NQO1). Detailed protocols of the assays for each enzyme are available in the Supporting Information.

Briefly, cells seeded in 96-well plates were exposed against 0.0003 to 80 µM 3-NBA for 24h. At the end of the exposure period, the medium was removed and the cells were washed three times with PBS before storage at -70°C. At the day of the experiment, the 96-well plates were thawed for 10 minutes before usage. Afterward, 100µL reaction mixture containing PBS or Tris as buffer, triton x-100 for cell lysis, and required cofactors and detection reagent for the corresponding enzyme, were added. The corresponding enzyme product was monitored by fluorescence or absorption measurement.

Determination of toxicological endpoints

Formation of reactive oxygen species (ROS)

ROS were detected by their reaction with the fluorescent indicator dye 2′,7′-dichloro-dihydrofluorescein diacetate (H_2DCF-DA; Life Technologies). Briefly, cells treated with normal cell culture medium were used to normalise between the independent experiments (n=5), while 50 µM of *tert*-butyl hydroperoxide served as positive control. After 24h of exposure, cells were washed three times with phosphate-buffered saline (37°C) and incubated with 10 µM H_2DCF-DA in PBS for 30 min at 37°C. Afterward, the cells were washed three times and the fluorescence was measured in PBS immediately at $\lambda_{(ex/em)}$ 485/535 nm.

Cell proliferation

Cell proliferation was monitored by incorporation of the thymidine analogue 5-ethynyl-2'-deoxyuridine (EdU, Santa Cruz Biotechnology) and detection with fluorescein-5-azide (FAM-

5-azide, Lumiprobe). 3.5 h before the end of the exposure period, 20 µL EdU labelling solution (10 µM/well) was added to each well and the exposure was continued for the remaining time. Afterwards, the culture medium was removed and the cells were washed twice with PBS followed by fixation for 15 minutes with 4% formaldehyde, 0.1% triton x-100 in PBS. To detect the incorporated EdU, the fixed cells were washed three times with PBS and incubated in a freshly prepared fluorescence labelling solution of 100 mM Tris-HCl (pH 8.0), 100 mM ascorbic acid, 1 mM $CuSO_4$ and 10 µM FAM-5-azide for 30 minutes. The fluorescence was monitored after three washing steps with PBS at $\lambda_{(ex/em)}$ 485/535 nm in PBS. Blank wells were used for background read-out, while unexposed cells were used to normalise the results between the independent experiments (n=5).

Mitochondrial membrane potential (MMP, Δψm)

Δψm was analysed by using the fluorescent mitochondrial membrane potential indicator rhodamin 123 (Rh123, Life Technologies). Cells treated with normal cell culture medium were used as negative controls while valinomycin (25µM) served as positive control. After exposure, the cells were washed three times with PBS (37°C) and incubated with 10 µM Rh123 for 30 min at 37°C. At the end of the incubation period, the dye solution was removed and the cells were washed twice with PBS (37°C) before measurement of the fluorescence intensity at $\lambda_{(ex/em)}$ 485/535 nm in PBS. Control cells were used to normalise the results between the independent experiments (n=5).

The cellular viability (MTT assay)

The viability respectively metabolic activity was determined by using the tetrazolium dye 3-(4,5-dimethylthiazol-2-yl)-2,5-diphenyltetrazolium bromide (MTT). Two hours before the end of the exposure period, 20 µL of a freshly prepared and sterile filtered MTT solution (5 mg/mL) was added to each well and mixed gently. Upon completion of the incubation, the culture medium was removed and the cells were washed twice with PBS. Cell lysis was performed with a mixture of 0.6 % glacial acetic acid, and 10 % SDS in DMSO. The mixture was added to each well (100 µL), and the plate was incubated for 5 min at RT, which was continued for 5 min on an orbital shaker. The cellular viability was determined by measurement of the absorbance at 492 nm to the reference wavelength of 620 nm. Blank wells were used for background read-out. Control cells were used to normalise the results between the independent experiments (n=5).

Glutathione quantification

Cellular glutathione (GSH) levels were measured by means of 5,5'-dithiobis-(2-nitrobenzoic acid) (DTNB, Ellman's reagent).[19,20] After exposure, the cells were washed three times with PBS before stored at -70°C. At the day of the experiment, the cells were thawed for 10 minutes at RT. Afterward, 100 µL of a reaction mixture (5 mM EDTA, 1 mM DTNB, 1 U/mL GSSG reductase, 0.6% sulfosalicylic acid, 0.2% Triton X-100 in PBS) was added and the plates were incubated for 5 minutes at RT. To initiate the reaction NADPH was added to each well (0.25 mM final conc. per well) and the absorbance were measured immediately at 415 nm for five minutes in one minute intervals.

To determine the cellular GSSG (glutathione disulphide) content, 1-methyl-2-vinylpyridinium triflate (M2VP, 20 µL/well of 3 mM solution in 0.2% Triton X-100) was added 2 minutes before the reaction mixture was added.

Calibration standards, GSH and GSSG, respectively, were treated similarly to the samples. The assay was performed four times (n=4) and the results were normalised to 10^6 cells.

Metabolomic profiling

Extraction of carbohydrate and lipid metabolites from cell lysates

The intermediates of energy metabolism were extracted by a methyl tert-butyl ether/methanol (MTBE/MeOH)-based technique.[21] Cells grown in a 75 cm^2 flask were exposed to five different concentrations of 3-NBA (0.3 nM, 10 nM, 80 nM, 10 µM and 80 µM) at 80 % confluence for 24h. At the end of the exposure, the cells were harvested according to standard procedures. The resulting cell pellet was washed three times with normal saline solution (isotonic saline solution, 0.9% NaCl) to remove remaining culture medium. During the last washing step, the cells were transferred to 2 mL reaction tubes for metabolite extraction. Cell lysis was performed by incubating the cells in a mixture of MTBE/MeOH (10:3, 400µL) by vortexing with 45 mg glass-beads (acid washed) for 2 minutes. The lysed cells were then centrifuged to separate the cell debris from the metabolites at 20,000 *xg* for 5 minutes at 4°C. The supernatant was removed and collected in 1.5 mL reaction tubes. The remaining pellet was re-extracted with 400 µL MTBE/MeOH (10:3) and the supernatants were combined. The separation of hydrophilic and lipophilic metabolites phase was induced by adding 200 µL water. After vortexing, the samples were centrifuged at 20,000 *xg* for 5 minutes at 4°C and the upper (organic) phase was transferred into a new 2 mL tube. The remaining aqueous phase was washed once with a water-saturated MTBE/MeOH solution (10:3:2.5; MTBE:MeOH:H_2O) and the organic phases were combined after centrifugation at 20,000 *xg*

for 5 minutes at 4°C. The aqueous phase was transferred into a GC-vial. Both metabolic fractions were dried in a vacuum centrifuge at RT.

Derivatisation of the metabolites

Aqueous fraction

50 µL of a 20 mg/mL solution of methoxyamine hydrochloride in pyridine was pipetted into the vial of the aqueous fraction and incubated at RT overnight (> 16h). Afterwards, 30 µL MSTFA was added and the fraction was further incubated for 30 minutes at 80°C

Organic fraction

100 µL toluene was added to the dried organic fraction, followed by 750 µL MeOH and 150 µL of an 8 % HCl solution in methanol. After each addition the samples were mixed. Afterwards, the samples were incubated overnight (> 16h) at RT to derivatised fatty acids to their corresponding methyl esters. At the end of incubation, the organic compounds were extracted by adding 150 µL hexane and 150 µL water. After centrifugation at 20,000 *xg* for 5 minutes at 4°C, the (upper) organic phase was transferred to a new vial and the aqueous phase was re-extracted with 150 µL. The organic phases were combined and dried in a vacuum centrifuge at RT. Finally, the dried sample was suspended in 50 µL pyridine and derivatised with 30 µL MSTFA for 30 min at 80°C.

GC/MS setup

The isolated and derivatised metabolites were identified and quantified by GC/MS analysis using an HP 6890/5973 GC/MS system (Agilent Technologies, Waldbronn, Germany). The instrument was equipped with a 30 m x 320 µm (i.d.) Optima 5 column coated with a 5% phenyl/95% methylpolysiloxane cross-linked stationary phase (0.25 µm film thickness; MACHEREY-NAGEL, Düren, Germany). Helium was used as carrier gas (flow rate of 1.5 mL/min). The analytes (1 µL each) were injected in the splitless mode with a solvent cut-off time of 6 minutes. The injector temperature was maintained at 280°C. The oven temperature was kept at 70°C for 1 min and then linearly increased at a rate of 1°C/min up to 76°C and from there at a rate of 6°C/min up to 300°C, where it was maintained for 5 min. The MS was operated in the electron impact ionisation mode at 70 eV with the quadrupole temperature set at 150°C and the source temperature at 230°C. Full scans were acquired by repetitively scanning over the mass range from 50 to 550 Da at a scan rate of 500 msec/scan.

GC/MS spectrum analysis

The resulting GC/MS spectra were deconvoluted with AMDIS (Automated Mass spectral Deconvolution and Identification System) and analysed with SpecConnect.[22] The resulting integrated signal matrix was used to calculate the metabolite ratios between the various groups and for statistical analysis using the KNIME Analytics Platform (ANOVA). The peak identification was performed with the GOLM metabolome database (Ver. 20111121),[23] and massbank.[24] The metabolite profiling was performed in four independent experiments (n=4). The resulting metabolites were annotated with ChEBI identifiers and submitted for enrichment analysis using MetaboAnalyst.[25] The STITCH v5.0 was used to investigate metabolite-protein interactions. The list of regulated metabolites was uploaded and the metabolic network was studied using STITCH v5.0. The network was computed under the assumption of a very high confidence interaction, > 0.9.[26]

Statistical analysis and multivariate analysis

All experiments were performed at least five times in independent runs unless otherwise stated. Microplate reader readouts of fluorescence or absorbance measurements were normalised to control wells. Control values were set to 100 %. Each analysis comprises three technical replicates. The level of statistical significance relative to control was calculated by using the analysis of variance (ANOVA) with Tukey's post-hoc test as a statistical method. The significance is represented in the graphs by asterisks (*, $p \leq 0.05$; **, $p \leq 0.01$; ***, $p \leq 0.001$).

Principal component analysis of the combined toxicological assays (activity and cytotoxicity assays) and GC-MS data supplemented with data from the combined toxicological assays (conc. 0.0003, 0.01, 0.08, 10 and 80 µM) was performed using the Multibase package (Numerical Dynamics, Japan).

RESULTS

Biotransformation of 3-NBA

Based on the intrinsic fluorescence of 3-ABA, one of the main metabolites of 3-NBA, the uptake, metabolic activation and its progress over 72 h were monitored. Exposure of RT4 cells to 17 different concentrations ranging from 0.0003 µM to 80 µM revealed a time- and dose-dependent increase in the cellular fluorescence intensity of 3-ABA compared to non-exposed cells. Elevated cellular fluorescence levels were detected for concentrations starting from 0.01 µM after 30 minutes of exposure. During the observation phase no saturation of fluorescence was detected (Fig. 1A). We assume that the trend of the reduced slope of the

fluorescence intensity after a longer exposure time reflects the depletion of 3-NBA in the culture medium, thus leading to a steady state of 3-ABA fluorescence.

The microscopic analysis of the cellular distribution of formed 3-ABA revealed a primary cytosolic localization of 3-ABA (Supporting Information, Fig. S1).

The analyses of the activity of phase-I and II enzymes revealed a non-monotonic dose-response which was mostly divided into three parts ranging from 0.0003 μM to 0.005 μM, 0.01 μM to 0.6 μM and 1.25 μM to 80 μM. The most pronounced activity alterations, in general, were observed for NQO1 (up to 122%), for XO (up to 105%) and a decrease for NATs to at least 88% (NAT1) respectively 90% (NAT2) (Fig. 1B).

The other activity assays, POR, CYP450, GST, and SULT1A, showed only minor alterations except for GST and SULT1A (Fig. 1B). They showed a concentration-dependent increase in activity at the highest exposure concentrations of 116% (SULT1A) and 118% (GST) compared to control.

Determination of toxicological endpoints

Various cellular endpoints were analysed to elucidate the cellular dose-response and to identify the beginning of disturbance in cellular homeostasis. The analysed toxicological endpoints showed a non-linear response to 3-NBA with partitions comparable to the shape of the dose-response curve of the metabolising enzymes.

ROS production and cell proliferation

The analysis of the cellular ROS levels revealed that at low exposure concentrations a slight decrease in ROS formation was observed, while at higher exposure concentrations, the cellular ROS increased up to 132 % when cells were treated with 0.01 μM to 10 μM. The maximal ROS level of 172 % was observed for 80 μM (Fig. 2A).

The proliferation rate showed a significant decrease, at the highest concentrations, of 14% as compared to control. However, at lower exposure concentrations no alterations were observed (Fig. 2B).

Mitochondrial membrane potential and cell viability

A significant increase in $\Delta\psi m$ was observed only for the highest exposure concentrations with levels from 110% (5 μM) to 118% (80 μM, Fig. 2D) as compared to the control.

The MTT assay as an indicator of cell viability exhibited a non-monotonic response in the exposure range from 0.0003 μM to 0.3 μM followed by a concentration-dependent decrease at

high 3-NBA dosages. The minimal cell viability was observed for 80 μM where the viability decreased to 64%, compared to the control levels (Fig. 2C).

Glutathione quantification

The determination of cellular glutathione levels revealed a concentration dependent significant increase in the total cellular content of glutathione from 0.147±0.014 mM in control cells to 0.215±0.018 mM when cells were exposed to 80 μM of 3-NBA. A similar result was obtained for oxidised glutathione which showed a concentration dependent significant increase from 4.4±2.6 μM in control to 25.4±2.6 μM when cells were exposed to 80 μM. The ratio of GSH to GSSG decreased from 32.33 in control to 7.47 in the cells exposed to 80 μM 3-NBA (Fig. 3).

Metabolomic profiling

Based on the results of the described assays, five different concentrations (0.0003 μM, 0.01 μM, 0.08 μM, 10 μM and 80 μM) were selected to observe changes in the cellular metabolism. The exposure to 3-NBA revealed various significantly altered cellular metabolites, 15 for cells exposed to 0.0003 μM (10 identified), 33 for 0.01 μM (28 identified), 183 for 0.08 μM (62 identified), 109 for 10 μM (36 identified) and 81 metabolites (43 identified) after the treatment with 80 μM. These metabolites fulfilled our criteria of an altered metabolite when compared to control (volcano plots of the metabolites are shown in Supporting Information, Fig. S4). A metabolite was considered altered when its relative abundance has changed by a factor not less than ± 1.5. The significantly altered and identified metabolites are listed in Supporting Information (Tabl. S1-5). The metabolites with altered concentrations include, among others, fatty acids (e.g. palmitic acid, oleic acid, linolenic acid), amino acids (e.g. glycine, serine, phenylalanine), substrates of glycolysis and TCA cycle (e.g. fructose-6-phosphate, citric acid) and antioxidant (hypotaurine, α-tocopherol). Enrichment analysis of the altered metabolites based on their ChEBi identifiers linked them to various metabolic pathways, among them pentose phosphate pathway, glutathione metabolism, glycolysis, gluconeogenesis, beta-oxidation of very long chain fatty acids, alpha-linolenic acid and linoleic acid metabolism (Fig. 4; Supporting Information Fig. S5-S9). The STITCH tool was used to provide a visualisation of predicted interactions of chemicals and proteins after exposure to 0.08 μM 3-NBA. The interaction network revealed that a large number of metabolites are linked to NADPH and 10-formyl-tetrahydrofolate (Fig. 5).

Multivariate analysis

The multivariate analysis of the obtained toxicological data including the data of the activity assays revealed three clusters for both principal component analyses. The software clustered the concentrations according to the cellular effect. The resulting groups consist of the concentrations 0.0003 to 0.02 μM (including control cells) cluster 1 and 0.04 to 10 μM cluster 2 and 80 μM cluster 3 (Fig. 6).

DISCUSSION

Found in diesel engine exhaust, which significantly contributes to air pollution, the nitrated polycyclic aromatic hydrocarbon 3-NBA is considered a suspected human carcinogen,[27] probably affecting the lungs. Studies have reported the presence of 3-ABA, the main metabolite of 3-NBA in urine samples of salt mine workers occupationally exposed to diesel engine exhaust.[16] Given that the bladder is the main organ where urine is stored, it is plausible to expect toxic effects on bladder epithelial cells, too. Therefore, the objective of the present study was to describe the dose-response behaviour of 3-NBA in vitro, and to elucidate the underlying cellular mechanisms. To reflect environmental condition, concentrations as low as 0.0003 μM 3-NBA, similar to 143 ng/24 h (1.5 L; 0.0004 μM 3-ABA) urine observed for 3-ABA,[16] were tested in the utilised cell model. In the high doses range, up to 10 μM was tested equivalent to ~ 3 mg/24 h urine. Due to the absence of strong toxic effects, a critical dose of 80 μM was tested although this concentration cannot be reached under environmental conditions.

The resulting data pointed to a non-linear effect with modest deviations from control conditions at low doses of 3-NBA and pronounced toxic effects at higher doses. At an intermediate level of exposure (0.04 – 10 μM 3-NBA, obtained by principal component analysis, additional processes were activated which became increasingly less effective in maintaining a controlled cellular state, as is evident for the obtained ROS results. Finally, pronounced toxic effects occurred at a concentration of 80 μM

Uptake and metabolic activation of 3-NBA into its toxic metabolite 3-ABA

An important determinant of the toxicity of a xenobiotic is the ability of a specific tissue to metabolise it. A suitable candidate for monitoring is 3-ABA, one of the main metabolites of 3-NBA, due to its auto-fluorescence. We could demonstrate that these cells were capable of metabolising 3-NBA into its toxic metabolite.[17,18,30,31] In our experimental setting, 3-ABA was detected as early as 30 minutes even in the cells exposed to low concentrations such as

0.01 µM 3-NBA. During the 72 h exposure, we observed a time-dependent accumulation of 3-ABA with no evidence of approaching saturation (Fig. 1A). Microscopic evaluation of the distribution within the cells revealed that 3-ABA was mainly found in the cytosol where the enzymes involved in the metabolism of 3-NBA are located.

So far, the bioactivation of 3-NBA has not been studied in detail in bladder cells. Therefore, the activity of a panel of enzymes - involved in the metabolism of 3-NBA - was measured. [32,33] The analysis revealed a high activity of NQO1 indicating that this enzyme might be the main contributor in metabolic conversion of 3-NBA in the utilized cell model, which is in agreement with previous studies (Fig. 1B).[36,37] The other enzymes, POR, XO, and CYP450 had an only negligible influence on bioactivation of 3-NBA. In addition, we also measured the activity of the conjugation enzymes NAT1/2 and SULT1A, which was reported to enhance the 3-NBA-derived DNA adduct formation.[38,33] However, treatment with 3-NBA only moderately influenced NAT1/2 by reducing their activity while SULT1A was only affected at the highest concentrations. The additionally performed test for GSTs, a key group of enzymes for cellular detoxification, showed an equal result. Interestingly, most described enzymes are regulated by the aryl hydrocarbon receptor (AhR) and polycyclic aromatic hydrocarbons are potent ligands for AhR. Nevertheless, the nitro-polycyclic aromatic hydrocarbon 3-NBA was not shown to induce these enzymes via AhR.[32–34]

Cytotoxicity of 3-NBA

After analysing the bioactivation of 3-NBA, we analysed the cytotoxic potential of 3-NBA within the wide concentration range used in this study (Fig. 2). To avoid interferences of 3-ABA auto-fluorescence at λ_{em} 550 to 700 nm, the fluorescence based toxicological assays were performed at excitation and emission wavelength λ_{ex} 488 nm and λ_{em} 535 nm.

ROS plays an important part in cellular stress response; in comparable studies a significant increase in ROS production was demonstrated, beginning at 0.01 µM 3-NBA in human alveolar cells (A549), and particularly 10 µM in RT4 cells, with both cell lines being exposed for 30 minutes.[37,39] In our model, treatment with 3-NBA induced a dose-dependent ROS production at a concentration of 0.01 µM. Nevertheless, compared to the above-mentioned studies, the increase in ROS production seemed to be less pronounced in our experimental setting, which might be due to the duration of the exposure. We assumed that within 30 minutes of exposure the cellular oxidative defence is not able to restore the cellular homeostasis as effectively as after an exposure of 24 h. After an increase of ROS the cells try to maintain a steady state, probably by activating specific pathways to face the increasing

oxidative stress, while their compensatory limit was exceeded when high concentrations of 80 µM was applied. This assumption is supported by our metabolomic data, described in detail in the "metabolomic profiling" section.

Furthermore, oxidative stress is closely intertwined with energy metabolism and, in particular, with mitochondrial activity. Measurement of cellular ATP levels (Supporting Information, Fig. S3) showed no perturbation over a wide concentration range, which was further confirmed by supportive $\Delta\psi m$ measurements. Alterations of both endpoints decreased ATP levels and hyperpolarisation of $\Delta\psi m$, were only observed for the higher dosages tested.

Metabolomic evaluation

Due to the complexity of this topic, we selected five concentrations based on the principal component analysis to compare different cellular states. This analysis grouped the concentrations according to the observed cellular effects i.e. 0.0003 to 0.02 µM (including control cells) as cluster 1, 0.04 to 10 µM as cluster 2 and 80 µM as cluster 3 (Fig. 6), out of which 0.0003, 0.01, 0.08, 10, and 80 µM were further selected for metabolomic analysis.

At lower concentrations of 3-NBA (0.0003 and 0.01 µM), several metabolites of pathways were altered which were associated with the antioxidant defence such as the taurine/hypotaurine, glutathione or vitamin B6 metabolism (Fig. 4).[40,41]

Exposure to 0.08 µM 3-NBA led to the regulation of the highest number of pathways indicating that the maintenance of the cellular homeostasis became increasingly challenging. Thus, 3-NBA impact on the protein biosynthesis, the amino sugar metabolisms or the pentose phosphate pathway might be a sign of the increasing cellular effort to provide energy and to face the disturbance of the redox state. Exposing the cells to 10 and 80 µM intensified the shift in energy metabolism, particularly towards the pentose phosphate pathway. The preference of the pentose phosphate pathway was also reported after the exposure to other xenobiotics such as iron, 4-monochlorobiphenyl or TCDD.[42–44]

A common toxic effect of these xenobiotics is an induction of oxidative stress, which can be counterbalanced by the glutathione system, which was also observed in our cell model (Fig. 3). Regeneration of oxidised glutathione is dependent on NADPH, which in turn is substantially produced in the oxidative pentose phosphate pathway. That and the additional generation of ribose 5-phosphate for the nucleotide synthesis make it perfectly understandable and obvious that the pentose phosphate pathway plays an important role in the redox defence and in the repair of DNA damage. In addition, the serine-driven one-carbon metabolism contributes markedly to the NADPH production. By the conversion of serine to glycine, the

methyl group is transferred to tetrahydrofolate, followed by oxidation to 10-formyl-tetrahydrofolate which is coupled to the reduction of $NADP^+$ to NADPH.[45] Accordingly, serine and glycine were increased after the exposure to 0.08 µM 3-NBA. The association network (Fig. 5), generated with STITCH, further highlights the connection between the altered metabolites, NADPH and 10-formyl-tetrahydrofolate.

Furthermore, 3-NBA also altered the fatty acid metabolism. Exposure to the lowest concentration already increased the levels of saturated fatty acids (palmitic acid, arachidic acid, behenic acid, lignoceric acid), which could be oxidised in the peroxisomes and mitochondria to fuel respiration. In addition, also polyunsaturated fatty acids (PUFAs) were mobilised. In this case, however, differences between the individual concentrations became apparent. Thus, levels of members of the n-6 family (γ-linolenic acid, arachidonic acid (AA)) were elevated in response to 0.01 and 0.08 µM 3-NBA while the n-3 fatty acids (α-linolenic acid, docosahexaenoic acid (DHA)) increased after treatment with 10 µM. In addition, AA and DHA serve as substrates for the downstream synthesis of lipid mediators, which modulate inter alia inflammation: those derived from n-6 PUFAs (AA) enhance, whereas n-3 PUFAs (DHA) derived mediators suppress this process.[46] Also in context with exposure to polycyclic aromatic hydrocarbons, the protective effect of n-3 PUFAs was recently reported.[47] In addition, PUFAs are a major determinant of the cellular membrane and therefore have a deep impact on mitochondrial function.[48] Thus, alterations of DHA or AA modulate ROS generation and interfere with the respiratory chain complex. Nevertheless, the direction of these modulations depends on many factors and requires further investigation.

In conclusion, the present study highlights the dose-response relationship of 3-NBA in bladder cancer cells regarding cytotoxicity, metabolising enzymes and the metabolomic state. Starting from a relevant environmental dose of 0.0003 µM up to 80 µM, we described the driving mechanism behind the different cellular states. Up to a concentration of 0.02 µM, 3-NBA exerted only low-dose effects given a functioning oxidative stress defence. In an intermediate exposure range from 0.04 µM to 10 µM, the cell increasingly utilised processes to protect the cells from the consequences of exposure. Higher doses of 3-NBA drove the cells irreversibly to a toxic state. The metabolomic data suggested that the pentose phosphate pathway and the folate metabolism play a leading role in the transition from an adaptive to an adverse cellular state. From the perspective of risk assessment, one might come to the cautious conclusion that the urinary concentration of exposed workers seemed to exert a low-dose effect. Nevertheless, this has to be further validated.

ASSOCIATED CONTENT

SUPPORTING INFORMATION

Methods and corresponding references of applied assays to determine enzyme activities of NQO1, CYP450, XO, POR, GST, SULT1A, NAT1 and NAT2; microscopic images of the cellular distribution of 3-ABA; bar graphs representation of the enzyme activity results and observed cellular ATP levels; volcano plot as graphical representation of the observed cellular metabolites by GC-MS; results of the enrichment analysis of significantly altered metabolites observed after exposure to 0.0003, 0.01, 0.08, 10 or 80 µM 3-NBA, by MetaboAnalyst; tables of significantly altered metabolites observed after exposure to 0.0003, 0.01, 0.08, 10 or 80 µM 3-NBA.

The Supporting Information is available free of charge via the Internet at http://pubs.acs.org.

AUTHOR INFORMATION

Corresponding Author

*E-mail: mario.pink@fau.de. Telephone: (+49) 9131-85-26102. Fax: (+49) 9131 -85-22317.

ORCID

Mario Pink: 0000-0002-5148-5138

Nisha Verma: 0000-0000-7558-167X

Funding

The authors acknowledge funding by the Deutsche Forschungsgemeinschaft (DFG) under Grant No. SCHM1207/5-1.

Conflict of interest

The authors declare no conflicts of interest.

ABBREVIATIONS

AA, arachidonic acid; 3-ABA, 3-aminobenzanthrone (3-amino-7H-benzo[*d,e*]anthracen-7-one); AMDIS, Automated Mass spectral Deconvolution and Identification System; ChEBI, Chemical Entities of Biological Interest; $CuSO_4$, copper sulphate; CYP450, cytochrome P450; DHA, docosahexaenoic acid; DMSO, dimethyl sulphoxide; EdU, 5-ethynyl-2'-deoxyuridine; FAM-5-azide, fluorescein-5-azide; GC-MS, gas chromatography-mass spectrometry; GSH,

glutathione; GSSG, glutathione disulphide; GST, glutathione S-transferase; H_2DCF-DA, 2′,7′-dichloro-dihydrofluorescein diacetate; MeOH, methanol; MMP, $\Delta\psi m$, mitochondrial membrane potential; MSTFA, N-methyl-N-(trimethylsilyl)trifluoroacetamide; MTBE, methyl *tert*-butyl ether; MTT, tetrazolium dye, 3-(4,5-dimethylthiazol-2-yl)-2,5-diphenyltetrazolium bromide; $NADP^+$, nicotinamide adenine dinucleotide phosphate, oxidised; NADPH, nicotinamide adenine dinucleotide phosphate, reduced; NAT, N-acetyltransferase isozyme; 3-NBA, 3-nitrobenzanthrone (3-nitro-7*H*-benzo[*d,e*]anthracen-7-one); NQO1, NAD(P)H:quinone oxidoreductase, PBS, phosphate buffered saline; POR, cytochrome P450 oxidoreductase; PUFA, polyunsaturated fatty acids, PPP, pentose phosphate pathway; Rh123, rhodamine 123; ROS, reactive oxygen species; RT, room temperature; SDS, sodium dodecyl sulphate; STITCH, Search Tool for Interactions of Chemicals; SULT1A1, sulfotransferase 1A1; TCA cycle, tricarboxylic acid cycle; XO, xanthine oxidase

REFERENCES

(1) Olfert, S. M., Felknor, S. A., and Delclos, G. L. (2006) An updated review of the literature: risk factors for bladder cancer with focus on occupational exposures. *South. Med. J. 99*, 1256–1263.
(2) Golka, K., Wiese, A., Assennato, G., and Bolt, H. M. (2003) Occupational exposure and urological cancer. *World J. Urol. 21*, 382–391.
(3) Bosetti, C., Boffetta, P., and Vecchia, C. L. (2007) Occupational exposures to polycyclic aromatic hydrocarbons, and respiratory and urinary tract cancers: a quantitative review to 2005. *Ann. Oncol. 18*, 431–446.
(4) Verma, N., Pink, M., Petrat, F., Rettenmeier, A. W., and Schmitz-Spanke, S. (2012) Exposure of primary porcine urothelial cells to benzo(a)pyrene: in vitro uptake, intracellular concentration, and biological response. *Arch. Toxicol. 86*, 1861–1871.
(5) Verma, N., Pink, M., Rettenmeier, A. W., and Schmitz-Spanke, S. (2013) Benzo[a]pyrene-mediated toxicity in primary pig bladder epithelial cells: A proteomic approach. *J. Proteomics 85*, 53–64.
(6) Verma, N., Pink, M., Petrat, F., Rettenmeier, A. W., and Schmitz-Spanke, S. (2015) Proteomic Analysis of Human Bladder Epithelial Cells by 2D Blue Native SDS-PAGE Reveals TCDD-Induced Alterations of Calcium and Iron Homeostasis Possibly Mediated by Nitric Oxide. *J. Proteome Res. 14*, 202–213.
(7) Bolt, H. M. (2014) Causation of human urothelial cancer: there are challenging new data! *Arch. Toxicol. 88*, 1769–1770.
(8) Kawanishi, M., Fujikawa, Y., Ishii, H., Nishida, H., Higashigaki, Y., Kanno, T., Matsuda, T., Takamura-Enya, T., and Yagi, T. (2013) Adduct formation and repair, and translesion DNA synthesis across the adducts in human cells exposed to 3-nitrobenzanthrone. *Mutat. Res. 753*, 93–100.
(9) Nagy, E., Adachi, S., Takamura-Enya, T., Zeisig, M., and Möller, L. (2006) DNA damage and acute toxicity caused by the urban air pollutant 3-nitrobenzanthrone in rats; Characterization of DNA adducts in eight different tissues and organs with synthesized standards. *Environ. Mol. Mutagen. 47*, 541–552.
(10) Nagy, E., Adachi, S., Takamura-Enya, T., Zeisig, M., and Möller, L. (2007) DNA adduct formation and oxidative stress from the carcinogenic urban air pollutant 3-nitrobenzanthrone and its isomer 2-nitrobenzanthrone, in vitro and in vivo. *Mutagenesis 22*, 135–145.
(11) Bieler, C. A., Cornelius, M. G., Stiborova, M., Arlt, V. M., Wiessler, M., Phillips, D. H., and Schmeiser, H. H. (2007) Formation and persistence of DNA adducts formed by the carcinogenic

air pollutant 3-nitrobenzanthrone in target and non-target organs after intratracheal instillation in rats. *Carcinogenesis 28*, 1117–1121.
(12) Arlt, V. M., Zhan, L., Schmeiser, H. H., Honma, M., Hayashi, M., Phillips, D. H., and Suzuki, T. (2004) DNA adducts and mutagenic specificity of the ubiquitous environmental pollutant 3-nitrobenzanthrone in Muta Mouse. *Environ. Mol. Mutagen. 43*, 186–195.
(13) Kanno, T., Kawanishi, M., Takamura-Enya, T., Arlt, V. M., Phillips, D. H., and Yagi, T. (2007) DNA adduct formation in human hepatoma cells treated with 3-nitrobenzanthrone: analysis by the 32P-postlabeling method. *Mutat. Res. 634*, 184–191.
(14) Enya, T., Suzuki, H., Watanabe, T., Hirayama, T., and Hisamatsu, Y. (1997) 3-Nitrobenzanthrone, a Powerful Bacterial Mutagen and Suspected Human Carcinogen Found in Diesel Exhaust and Airborne Particulates. *Environ. Sci. Technol. 31*, 2772–2776.
(15) IARC Evaluation of Carcinogenic Risk to Humans. (2014) 3-NITROBENZANTHRONE, in *IARC Monographs on the Evaluation of Carcinogenic Risks to Humans, No. 105.*
(16) Seidel, A., Dahmann, D., Krekeler, H., and Jacob, J. (2002) Biomonitoring of polycyclic aromatic compounds in the urine of mining workers occupationally exposed to diesel exhaust. *Int. J. Hyg. Environ. Health 204*, 333–338.
(17) Chen, G., Lambert, I. B., Douglas, G. R., and White, P. A. (2005) Assessment of 3-nitrobenzanthrone reductase activity in mammalian tissues by normal-phase HPLC with fluorescence detection. *J. Chromatogr. B 824*, 229–237.
(18) Murahashi, T., Watanabe, T., Otake, S., Hattori, Y., Takamura, T., Wakabayashi, K., and Hirayama, T. (2003) Determination of 3-nitrobenzanthrone in surface soil by normal-phase high-performance liquid chromatography with fluorescence detection. *J. Chromatogr. A 992*, 101–107.
(19) Rahman, I., Kode, A., and Biswas, S. K. (2007) Assay for quantitative determination of glutathione and glutathione disulfide levels using enzymatic recycling method. *Nat. Protoc. 1*, 3159–3165.
(20) Vandeputte, C., Guizon, I., Genestie-Denis, I., Vannier, B., and Lorenzon, G. (1994) A microtiter plate assay for total glutathione and glutathione disulfide contents in cultured/isolated cells: performance study of a new miniaturized protocol. *Cell Biol. Toxicol. 10*, 415–421.
(21) Pink, M., Verma, N., Rettenmeier, A. W., and Schmitz-Spanke, S. (2014) Integrated proteomic and metabolomic analysis to assess the effects of pure and benzo[a]pyrene-loaded carbon black particles on energy metabolism and motility in the human endothelial cell line EA.hy926. *Arch. Toxicol. 88*, 913–934.
(22) Styczynski, M. P., Moxley, J. F., Tong, L. V., Walther, J. L., Jensen, K. L., and Stephanopoulos, G. N. (2007) Systematic identification of conserved metabolites in GC/MS data for metabolomics and biomarker discovery. *Anal. Chem. 79*, 966–973.
(23) Kopka, J., Schauer, N., Krueger, S., Birkemeyer, C., Usadel, B., Bergmüller, E., Dörmann, P., Weckwerth, W., Gibon, Y., Stitt, M., Willmitzer, L., Fernie, A. R., and Steinhauser, D. (2005) GMD@CSB.DB: the Golm Metabolome Database. *Bioinforma. Oxf. Engl. 21*, 1635–1638.
(24) Horai, H., Arita, M., Kanaya, S., Nihei, Y., Ikeda, T., Suwa, K., Ojima, Y., Tanaka, K., Tanaka, S., Aoshima, K., Oda, Y., Kakazu, Y., Kusano, M., Tohge, T., Matsuda, F., Sawada, Y., Hirai, M. Y., Nakanishi, H., Ikeda, K., Akimoto, N., Maoka, T., Takahashi, H., Ara, T., Sakurai, N., Suzuki, H., Shibata, D., Neumann, S., Iida, T., Tanaka, K., Funatsu, K., Matsuura, F., Soga, T., Taguchi, R., Saito, K., and Nishioka, T. (2010) MassBank: a public repository for sharing mass spectral data for life sciences. *J. Mass Spectrom. JMS 45*, 703–714.
(25) Xia, J., Sinelnikov, I. V., Han, B., and Wishart, D. S. (2015) MetaboAnalyst 3.0—making metabolomics more meaningful. *Nucleic Acids Res. 43*, W251-257.
(26) Szklarczyk, D., Santos, A., von Mering, C., Jensen, L. J., Bork, P., and Kuhn, M. (2016) STITCH 5: augmenting protein–chemical interaction networks with tissue and affinity data. *Nucleic Acids Res. 44*, D380–D384.
(27) Benbrahim-Tallaa, L., Baan, R. A., Grosse, Y., Lauby-Secretan, B., Ghissassi, F. E., Bouvard, V., Guha, N., Loomis, D., and Straif, K. (2012) Carcinogenicity of diesel-engine and gasoline-engine exhausts and some nitroarenes. *Lancet Oncol. 13*, 663–664.
(28) Calabrese, E. J., and Baldwin, L. A. (2001) Hormesis: U-shaped dose responses and their centrality in toxicology. *Trends Pharmacol. Sci. 22*, 285–291.
(29) Zhang, Q., Pi, J., Woods, C. G., Jarabek, A. M., Clewell, H. J., and Andersen, M. E. (2008) Hormesis and Adaptive Cellular Control Systems. *Dose-Response 6*, 196–208.

(30) Kalnina, I., Klimkane, L., Kirilova, E., Toma, M. M., Kizane, G., and Meirovics, I. (2007) Fluorescent Probe ABM for Screening Gastrointestinal Patient's Immune State. *J. Fluoresc. 17*, 619–625.
(31) Kalnina, I., Bruvere, R., Zvagule, T., Gabruseva, N., Klimkane, L., Kirilova, E., Meirovics, I., and Kizane, G. (2010) Fluorescent Probe ABM and Estimation of Immune State in Patients with Different Pathologies (Review Article). *J. Fluoresc. 20*, 9–17.
(32) Arlt, V. M. (2005) 3-Nitrobenzanthrone, a potential human cancer hazard in diesel exhaust and urban air pollution: a review of the evidence. *Mutagenesis 20*, 399–410.
(33) Stiborová, M., Frei, E., Schmeiser, H. H., Arlt, V. M., and Martínek, V. (2014) Mechanisms of Enzyme-Catalyzed Reduction of Two Carcinogenic Nitro-Aromatics, 3-Nitrobenzanthrone and Aristolochic Acid I: Experimental and Theoretical Approaches. *Int. J. Mol. Sci. 15*, 10271–10295.
(34) Øvrevik, J., Arlt, V. M., Øya, E., Nagy, E., Mollerup, S., Phillips, D. H., Låg, M., and Holme, J. A. (2010) Differential effects of nitro-PAHs and amino-PAHs on cytokine and chemokine responses in human bronchial epithelial BEAS-2B cells. *Toxicol. Appl. Pharmacol. 242*, 270–280.
(35) Chen, G., Gingerich, J., Soper, L., Douglas, G. R., and White, P. A. (2008) Tissue-specific metabolic activation and mutagenicity of 3-nitrobenzanthrone in Muta^{TM}Mouse. *Environ. Mol. Mutagen. 49*, 602–613.
(36) Krais, A. M., Mühlbauer, K.-R., Kucab, J. E., Chinbuah, H., Cornelius, M. G., Wei, Q.-X., Hollstein, M., Phillips, D. H., Arlt, V. M., and Schmeiser, H. H. (2015) Comparison of the metabolic activation of environmental carcinogens in mouse embryonic stem cells and mouse embryonic fibroblasts. *Toxicol. In Vitro 29*, 34–43.
(37) Reshetnikova, G., Sidorenko, V. S., Whyard, T., Lukin, M., Waltzer, W., Takamura-Enye, T., and Romanov, V. (2016) Genotoxic and cytotoxic effects of the environmental pollutant 3-nitrobenzanthrone on bladder cancer cells. *Exp. Cell Res. 349*, 101–108.
(38) Arlt, V. M., Meinl, W., Florian, S., Nagy, E., Barta, F., Thomann, M., Mrizova, I., Krais, A. M., Liu, M., Richards, M., Mirza, A., Kopka, K., Phillips, D. H., Glatt, H., Stiborova, M., and Schmeiser, H. H. (2016) Impact of genetic modulation of SULT1A enzymes on DNA adduct formation by aristolochic acids and 3-nitrobenzanthrone. *Arch. Toxicol.* 1–19.
(39) Hansen, T., Seidel, A., and Borlak, J. (2007) The environmental carcinogen 3-nitrobenzanthrone and its main metabolite 3-aminobenzanthrone enhance formation of reactive oxygen intermediates in human A549 lung epithelial cells. *Toxicol. Appl. Pharmacol. 221*, 222–234.
(40) Fontana, M., Amendola, D., Orsini, E., Boffi, A., and Pecci, L. (2005) Oxidation of hypotaurine and cysteine sulphinic acid by peroxynitrite. *Biochem. J. 389*, 233–240.
(41) Depeint, F., Bruce, W. R., Shangari, N., Mehta, R., and O'Brien, P. J. (2006) Mitochondrial function and toxicity: Role of B vitamins on the one-carbon transfer pathways. *Chem. Biol. Interact. 163*, 113–132.
(42) Budak, H., Ceylan, H., Kocpinar, E. F., Gonul, N., and Erdogan, O. (2014) Expression of Glucose-6-Phosphate Dehydrogenase and 6-Phosphogluconate Dehydrogenase in Oxidative Stress Induced by Long-Term Iron Toxicity in Rat Liver. *J. Biochem. Mol. Toxicol. 28*, 217–223.
(43) Xiao, W., Sarsour, E. H., Wagner, B. A., Doskey, C. M., Buettner, G. R., Domann, F. E., and Goswami, P. C. (2014) Succinate dehydrogenase activity regulates PCB3-quinone-induced metabolic oxidative stress and toxicity in HaCaT human keratinocytes. *Arch. Toxicol. 90*, 319–332.
(44) Nault, R., Fader, K. A., Kirby, M. P., Ahmed, S., Matthews, J., Jones, A. D., Lunt, S. Y., and Zacharewski, T. R. (2016) Pyruvate Kinase Isoform Switching and Hepatic Metabolic Reprogramming by the Environmental Contaminant 2,3,7,8-Tetrachlorodibenzo-p-Dioxin. *Toxicol. Sci. 149*, 358–371.
(45) Fan, J., Ye, J., Kamphorst, J. J., Shlomi, T., Thompson, C. B., and Rabinowitz, J. D. (2014) Quantitative flux analysis reveals folate-dependent NADPH production. *Nature 510*, 298–302.
(46) Assies, J., Mocking, R. J. T., Lok, A., Ruhé, H. G., Pouwer, F., and Schene, A. H. (2014) Effects of oxidative stress on fatty acid- and one-carbon-metabolism in psychiatric and cardiovascular disease comorbidity. *Acta Psychiatr. Scand. 130*, 163–180.
(47) Gdula-Argasińska, J., Czepiel, J., Totoń-Żurańska, J., Wołkow, P., Librowski, T., Czapkiewicz, A., Perucki, W., Woźniakiewicz, M., and Woźniakiewicz, A. (2016) n-3 Fatty acids regulate the

inflammatory-state related genes in the lung epithelial cells exposed to polycyclic aromatic hydrocarbons. *Pharmacol. Rep. 68*, 319–328.

(48) Rohrbach, S. (2009) Effects of Dietary Polyunsaturated Fatty Acids on Mitochondria. *Curr. Pharm. Des. 15*, 4103–4116.

Figure 1: Determination of 3-ABA accumulation and analysis of enzyme activities. (**A**) Determination of the metabolic activation of 3-NBA to 3-ABA over 72 h. The intrinsic fluorescence of 3-ABA (λ_{ex} 485 nm, λ_{em} 595 nm) was used to monitor the metabolic activation and its progress. Elevated fluorescence levels were observed starting from 0.1 µM and 30 minutes of exposure. At lower exposure concentrations no increase in fluorescence could be measured. During the measurement, no saturation in 3-ABA fluorescence was observed.

(**B**) Heat map illustration of the measured enzyme activities. The activity of enzymes reported to be involved in metabolic activation of 3 NBA, NQO1, POR, XO and CYP450 and conjugation, NAT1 and 2, SULT1A and GST as an important enzyme in detoxification, were tested after exposure to 3-NBA for 24 h. The represented data in the heat map are average values of 7 independent experiments; bar graphs to each tested enzyme were shown in Supporting Information (Fig. S2).

Figure 2: Determination of 3-NBA cytotoxicity. Cytotoxic effects caused by 3-NBA after 24 h exposure was monitored by measuring alterations of cellular ROS levels (A) and proliferation (EdU, B), cell viability (MTT, C) and mitochondrial membrane potential (MMP, D). All measured toxicological endpoints exerted a non-monotonic response to 3-NBA with modest alteration up 0.001 μM, an intermediate range of response between 0.004 and 10 μM and a toxic response after treatment with 80 μM. The obtained values were normalised to controls (n = 5; *, $p<0.05$).

Figure 3: Glutathione quantification. After 24 h of exposure with 3-NBA, the GSH content was quantified by means of DTNB (Ellman's reagent). The measurements were performed by using a microplate reader (OD_{412nm}). The data were presented as mean ± SEM of four independent experiments. The level of significance relative to control was determined by using the t-test (*, $p \leq 0.05$; **, $p \leq 0.01$).

Figure 4: Cumulative representation of the enrichment analysis. The graphs illustrate signalling pathways that are enriched on the basis of the metabolites passing the filtering criteria. The corresponding metabolites are listed in Supporting Information (Tabl. S1-5). The bars indicate the degree of enrichment of the specific pathway. The analysis highlighted the shift in cellular metabolism when exposed to higher dosages of 3-NBA. Starting at an exposure to 0.08 µM 3-NBA, the cells re-schedule the cellular metabolism towards protein biosynthesis, the amino sugar metabolisms or the pentose phosphate pathway. This metabolic shift might be a sign of the increasing cellular effort to maintain homeostasis by the generation of redox equivalents and to provide substances for cell repair, lipids, and backbones for nucleotides.

Figure 5: Stitch annotation network based on the altered metabolites observed after exposure to 0.08 μM 3-NBA. The network computed under the assumption of very high confidences interactions, > 0.9, with 1 being the highest possible confidence. The network shows strong interactions between the observed metabolites, 10-formyl-tetrahydrofolate and NADPH. Functional enrichments of the network assigned them to one-carbon metabolic process and tetrahydrofolate interconversion/metabolism.

Figure 6: Principal component analysis of the obtained data. The analysis was performed to discriminate for concentration-dependent differences in the cellular behaviour. Two analysis were performed, once based on the GC-MS data supplemented with data from the monitored toxicological endpoints and activity assays (**A**, conc. 0.0003, 0.01, 0.08, 10 and 80 µM) and a second time for all tested concentrations based on toxicological endpoint and activity assay results (**B**). The analysis discriminates in both analyses three clusters of concentrations based on their cellular behaviour. Categorised in the first cluster are (cluster 1) concentrations ranging from 0.0003 µM to 0.02 µM including control, categorised in the second cluster are concentrations ranging from 0.04 µM to 10 µM (cluster 2) and in the third cluster 80 µM (cluster 3).

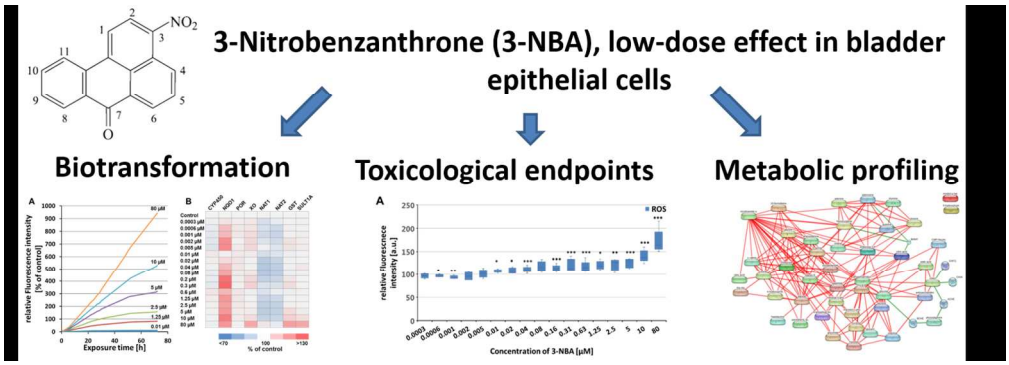

Table of Content

272x96mm (150 x 150 DPI)

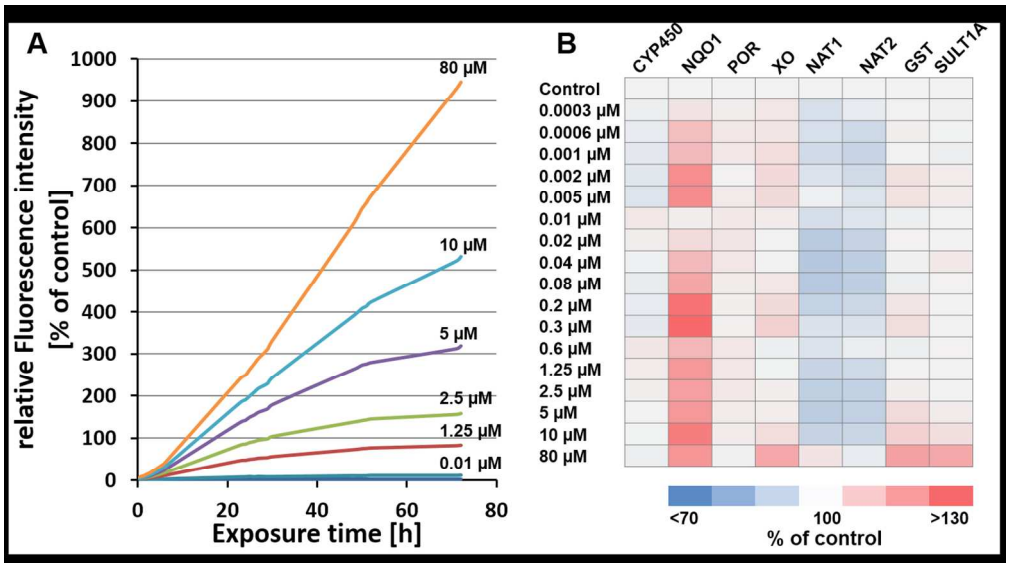

Figure 1

246x137mm (150 x 150 DPI)

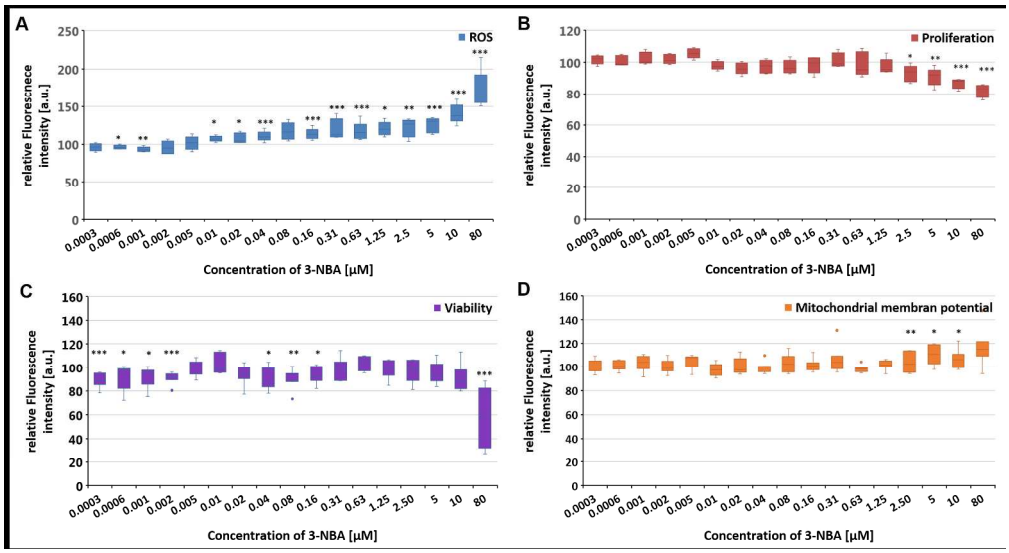

Figure 2

454x247mm (150 x 150 DPI)

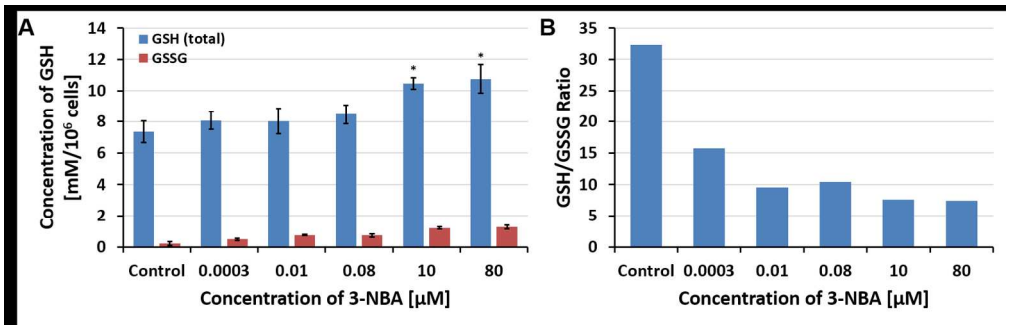

Figure 3

307x97mm (150 x 150 DPI)

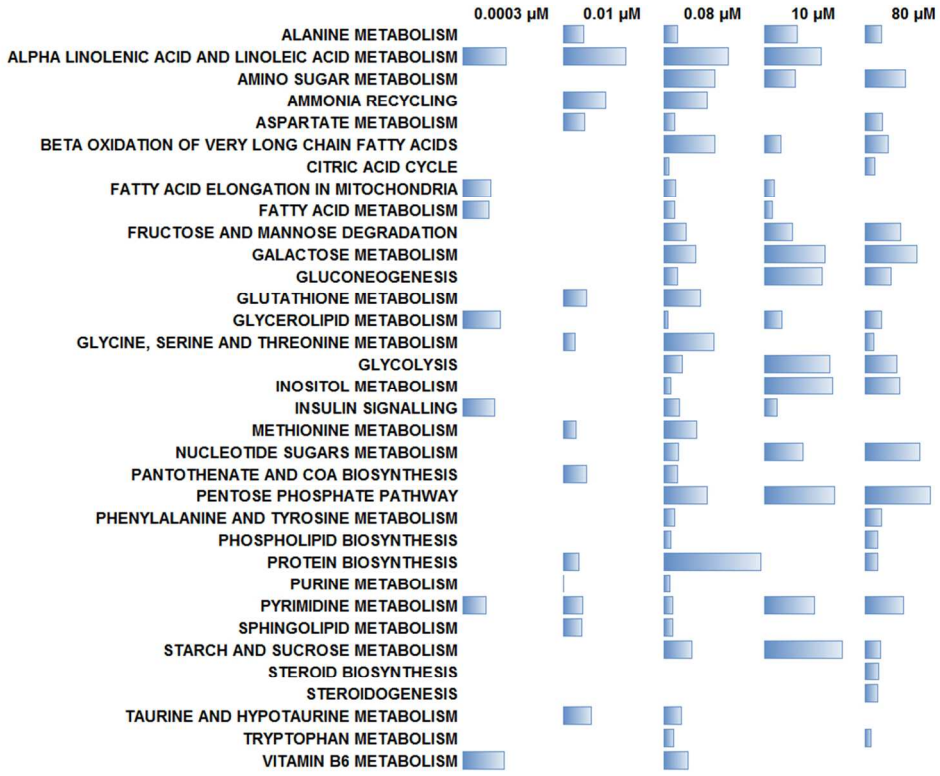

Figure 4

276x212mm (96 x 96 DPI)

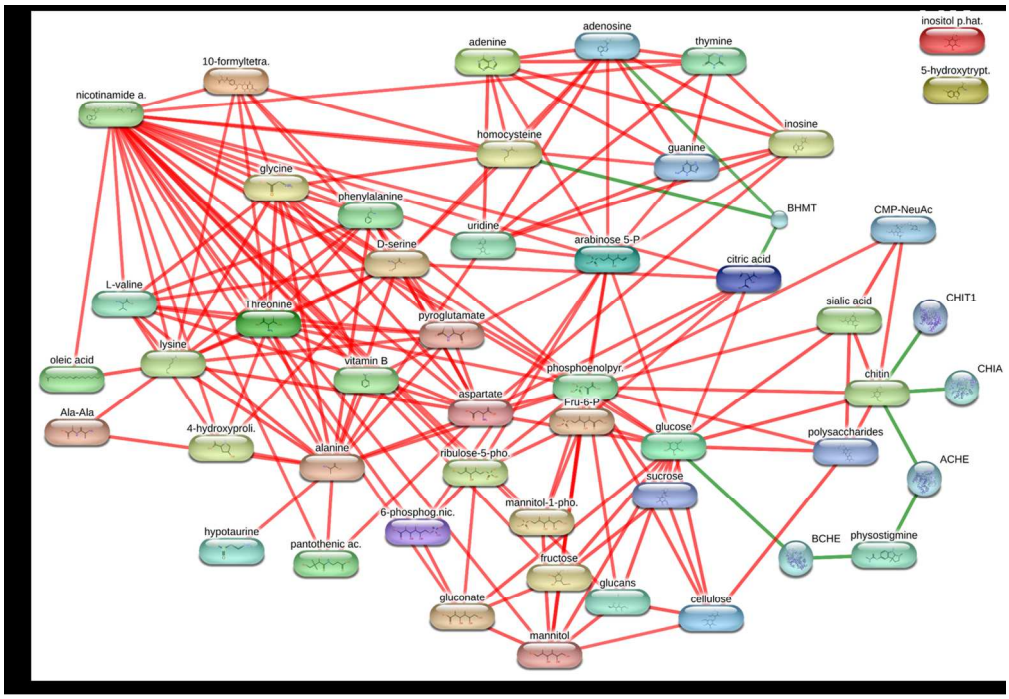

Figure 5

254x174mm (150 x 150 DPI)

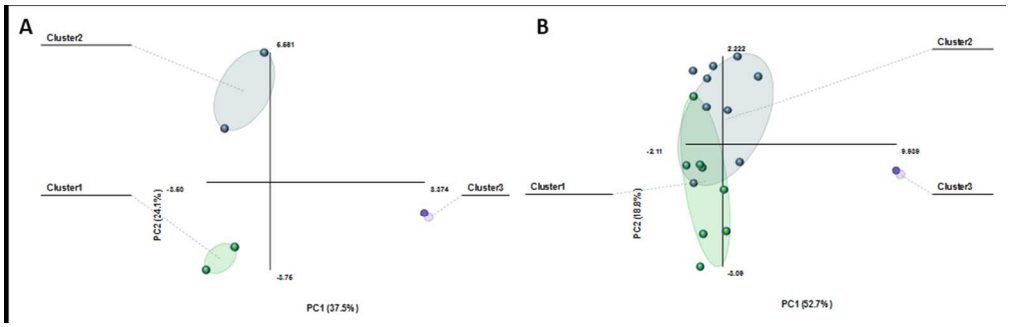

Figure 6

169x53mm (150 x 150 DPI)